catalysts

MDPI

Article

On the Oxygen Reduction Reaction Mechanism Catalyzed by Pd Complexes on 2D Carbon. A Theoretical Study

Marco Bonechi [1], Walter Giurlani [1,2], Martina Vizza [1], Matteo Savastano [1], Andrea Stefani [3], Antonio Bianchi [1,4], Claudio Fontanesi [5] and Massimo Innocenti [1,2,4,6,*]

[1] Department of Chemistry "Ugo Schiff", University of Florence, Via della Lastruccia 3, 50019 Sesto Fiorentino, Italy; marco.bonechi1@stud.unifi.it (M.B.); walter.giurlani@unifi.it (W.G.); martina.vizza@unifi.it (M.V.); matteo.savastano@unifi.it (M.S.); antonio.bianchi@unifi.it (A.B.)
[2] National Interuniversity Consortium of Materials Science and Technology (INSTM), Via G. Giusti 9, 50121 Firenze, Italy
[3] Department of Physics, Università Degli Studi di Modena e Reggio Emilia, Via Campi 213, 41125 Modena, Italy; andrea.stefani@unimore.it
[4] Center for Colloid and Surface Science (CSGI), Via della Lastruccia 3, 50019 Sesto Fiorentino, Italy
[5] Department of Engineering "Enzo Ferrari", DIEF, Università Degli Studi di Modena e Reggio Emilia, Via Vivarelli 10, 41125 Modena, Italy; claudio.fontanesi@unimore.it
[6] Insititute of Chemistry of Organometallic Compounds (ICCOM), National Research Council (CNR), Via Madonna del Piano 10, 50019 Sesto Fiorentino, Italy
* Correspondence: minnocenti@unifi.it

Citation: Bonechi, M.; Giurlani, W.; Vizza, M.; Savastano, M.; Stefani, A.; Bianchi, A.; Fontanesi, C.; Innocenti, M. On the Oxygen Reduction Reaction Mechanism Catalyzed by Pd Complexes on 2D Carbon. A Theoretical Study. *Catalysts* **2021**, *11*, 764. https://doi.org/10.3390/catal11070764

Academic Editors: Jaroslaw Polanski, Piotr Bartczak and Tomasz Siudyga

Received: 11 June 2021
Accepted: 23 June 2021
Published: 24 June 2021

Abstract: Oxygen Reduction Reaction (ORR) is the bottle-neck strategic reaction ruling the fuel cell efficiency process. The slow kinetics of the reaction require highly effective electrocatalysts for proper boosting. In this field, composite catalysts formed by carbon nanotubes functionalized with palladium(II) complexes showed surprising catalytic activity comparable to those of a commercial Pt electrode, but the catalytic mechanisms of these materials still remain open to discussion. In this paper, we propose the combination of experimental and theoretical results to unfold the elementary reaction steps underlying the ORR catalysis.

Keywords: fuel cell; ORR; PM6; band-gap; 2D carbon catalyst; SACs

1. Introduction

In recent years, issues concerning the energy sector have been at the focus of international discussions; the progressive depletion of fossil reserves and the increase in energy demand have led to the rise in fuel and electricity prices. Moreover, we are witnessing an increasing attention to pollution and environmental impact. New stricter standards for vehicle emissions are directing manufacturers to find new systems for energy production and storage. In this context, fuel cells are promising candidates for a sustainable future. The oxygen reduction reaction (ORR) is one of the most studied reactions in the field of energy. This reaction allows the release of chemical energy stored in the vector molecule H_2 in the form of electricity without producing any waste. For this reason, ORR is regarded as a highly strategic reaction. The oxygen reduction reaction can take place in two main ways: from a direct reduction to water (H_2O), with the exchange of 4 electrons per oxygen molecule or from an intermediate reduction to hydrogen peroxide (H_2O_2), with the exchange of two electrons. The slow kinetics of the reaction constitutes the theoretical and practical limit to its use in the energy sector. The use of a cathode catalyst is mandatory to achieving a satisfying ORR conversion rate; in fact, it is very difficult to electrochemically break the O_2 bond, which has an exceptionally strong bond energy. Many types of catalysts have been developed in order to improve kinetics and achieve better efficiencies. Semi-empirical quantum mechanical based methods offer the possibility to derive useful

information for understanding the reaction mechanism and evaluate different conformational structures, complexation energies, and species interaction energies [1]. The study of the energy levels of molecular orbitals allows the understanding of the phenomena of charge transfer and electrical reduction [2]. This kind of information allows one to evaluate the different reactivity of catalysts. Currently, platinum-based compounds show the best catalytic activity; however, the cost of this metal limits large-scale commercialization. For this reason, alternative catalysts are being experimented on, in which attempts are made to reduce the content of so-called Pt group metals (PGMs) or to replace them with a less precious metal [3–5]. Several substrates have been proposed as possible solid supports, among which are many carbon-based materials, including a new class of green catalysts made by pyrolysis of waste materials such as tires [6–9]. Carbon nanotubes (CNTs) have gathered a lot of attention in recent years due to their peculiar chemical and physical properties that make them suitable for catalytic processes [10]. They show a graphitic conductivity that can occur both in the plane of the π orbitals and inside the nanotube itself and do not show heating effects as a result of a current flow. Noncovalent functionalization approach offers the possibility to keep composite systems together, preserving the electrical properties of CNTs. CNTs-Pd(II) complexes have been used to prepare functionalized surfaces and working electrodes, which proved to be effective in catalyzing the ORR process [3,4,11]. Thus, in this paper, we aim to rationalize the catalytic role of such a class of composite catalysts. The latter showed surprising catalytic activity in ORR: MWCNTs/HL1-Pd(II), (Cat1), and MWCNTs/HL2-Pd(II) (Cat2) [11].

2. Oxygen Reduction Reaction: ORR

The two studied catalysts consist of carbon nanotubes functionalized with two different ligands, which are adsorbed on the nanotube surface by π-π stacking interactions. The two different ligands employed (HL1 and HL2) are organic molecules consisting of three main moieties: a pyrimidine group, which serves as the anchoring site, an aliphatic carbon spacer, and a terminal macrocycle. The latter acts as an organic ligand able to form a stable complex with the Pd(II) cation. HL1 has a shorter spacer group than HL2: $-(CH_2)_2-$ and $-(CH_2)_3-NH-(CH_2)_2-$, respectively. Experimentally, Cat1 and Cat2 were obtained through a supramolecular approach [12]. Moreover, adsorption of the catalyst, through the pyrimidine ligands on the graphitic surface, allows one to obtain active sites consisting of a single metal ion, implying a significant reduction of precious metal mass. Within the catalyst structure, the Pd(II) cation is coordinated by three nitrogen atoms from the macrocycle, and one hydroxide (OH^-) anion (provided from the bulk alkaline solution where the ORR process is carried out). The terminal macrocycle behaves as a tridentate ligand, leaving an active position in the first coordination sphere of Pd(II); in this way, the uptake of an oxygen molecule is assisted. Both systems have quite positive onset potential (vs. RHE) with a four electrons overall reduction process, eventually leading to the direct production of water (a significant reduction of hydrogen peroxide, a dangerous side-reaction byproduct, concentration is also observed experimentally [11]). Cat2 has the best catalytic activity, especially with regard to reduced production of hydrogen peroxide; we are led to believe that the longer spacer of HL2 produces a brush-like arrangement of the catalytic sites that promotes the capture of gaseous reactants from solution.

ORR in alkaline media is rationalized by a four steps $4e^-$ electron reduction mechanism, as originally proposed by Latimer [13–15]. In general, the overall reaction, (1), emerges as the combination of different elementary steps; see, for instance, Reactions (2) and (3). Disproportionation Reaction (4), as well as adsorption of the hydroxyl anion, play a role too [16].

$$O_2 + 2H_2O + 4e^- \rightarrow 4OH^- \; E = +0.401 \; V \; vs. \; NHE \quad (1)$$

$$O_2 + H_2O + 2e^- \rightarrow HO_2^- + OH^- \; E = -0.065 \; V \; vs. \; NHE \quad (2)$$

$$HO_2^- + H_2O + 2e^- \rightarrow 3OH^- \; E = +0.867 \; V \; vs. \; NHE \quad (3)$$

$$HO_2^- \rightarrow 2OH^- + O_2 \quad (4)$$

Thus, the kinetics of the oxygen reduction reaction depends on a quite complex reaction mechanism, involving a number of side-reaction intermediates as well as physical adsorption steps reactions from (5) to (9) (vide infra). As a final result, the ORR acts as the rate determining step in the water splitting [17–20].

$$O_2 \rightarrow O_{2(ads)} \tag{5}$$

$$O_{2(ads)} + H_2O + e^- \rightarrow OOH_{(ads)} + OH^- \tag{6}$$

$$OOH_{(ads)} + e^- \rightarrow O_{(ads)} + OH^- \tag{7}$$

$$O_{(ads)} + H_2O + e^- \rightarrow OH_{(ads)} + OH^- \tag{8}$$

$$OH_{(ads)} + e^- \rightarrow OH^- \tag{9}$$

Equations (5)–(9) form the 4-electron reduction pathway, resulting in the production of four OH^- ions. Then, as an alternative to Reaction (7), OOH radical can be further reduced, eventually desorbing as a peroxide anion OOH^- Equation (10).

$$OOH_{(ads)} + e^- \rightarrow OOH^- \tag{10}$$

In the case of (10) as the end of the reaction chain, an overall two-electron reaction mechanism is obtained. The latter is claimed to be the effective pathway when using carbon based materials for the ORR, such as carbon nanotubes (MWCNTs) [21]. Indeed, in the case of single-atom catalysts (SACs), i.e., the class of compounds formed by carbon nanotubes functionalized with Pd(II) complexes, experimental evidence indicates that the main ORR reaction path involves the oxygen reduction mediated by Pd(II), eventually following a four-electron reaction mechanism. In this case, an associative mechanism involving direct contact between O_2 and the Pd(II) complex is assumed [3,4,11]. Thus, based on the already accepted ORR mechanism catalyzed by transition metal complexes in acidic media [22], we propose for the alkaline media a set of elementary reactions, from (11) to (13). Where: L represents the ligand and Me is the metal:

$$\left[LMe^{II}\right] + O_2 \rightleftharpoons \left[LMe^{\delta+} \ldots O_2^{\delta-}\right] \tag{11}$$

$$\left[LMe^{\delta+} \ldots O_2^{\delta-}\right] + H_2O \rightarrow \left[LMe^{III} \ldots OOH\right]^+ + OH^- \tag{12}$$

$$\left[LMe^{III} \ldots OOH\right]^+ + 2e^- \rightarrow \left[LMe^{II} \ldots O\right] + OH^- \tag{13}$$

We propose the further set of elementary steps, which is consistent with the final ORR process:

$$\left[LMe^{II} \ldots O\right] + H_2O \rightarrow \left[LMe^{III} \ldots OH\right]^+ + OH^- \tag{14}$$

$$\left[LMe^{III} \ldots OH\right]^+ + 2e^- \rightarrow \left[LMe^{II}\right] + OH^- \tag{15}$$

In particular, Reaction (16) eventually gives due count to the formation of the peroxide anion, as it is reported in the literature [17,18,23].

$$\left[LMe^{III} \ldots OHH\right]^+ + 2e^- \rightarrow \left[LMe^{II}\right] + OHH^- \tag{16}$$

3. Results and Discussion

The calculation of the electrochemical redox properties followed a heuristic approach. Systems of different complexity for Cat1 and Cat2 were considered; the ligand structure (HL1/HL2) had been optimized as a single molecule, then the complexed Pd(II) cation

and its counterion (OH^-) were subsequently introduced, followed by the C2D moiety and the oxygen molecule. HL1 and HL2 are structurally related compounds, as can be seen in Figures 1 and 2.

Figures 3 and 4 show potential energy surfaces relevant to the combination of the different moieties (i.e., reaction path), which concur to form the complete Cat1 and Cat2 catalyst. The energy pattern found in Figures 3 and 4 gives due count to the spontaneous (down-hill in energy) stabilizing interaction between the Pd(II) complexes and the C2D moiety (which simulates the CNT). Remarkably, the HL2/C2D energy stabilization is larger than that corresponding to the HL1/C2D one. Moreover, Cat2 shows the highest oxygen interaction energy. With the energy values obtained, we can state that the oxygen molecule does not replace the hydroxyl anion (as previously assumed) but is coordinated by Pd(II) in the apical position. This information is especially interesting in terms of catalyst design. While the presence of an ancillary fast-exchangeable ligand (Cl^-) was essential for Sonogashira cross-coupling [12,24], as the process requires simultaneous coordination of two different reagents on Pd(II), this is not mandatory for ORR, as O_2 is able to form an apical bond on the d^8 metal center anyway. This could pave the way to direct usage of Pd(II) square planar complexes with tetradentated ligands. Interaction energies for Cat1 and Cat2 are listed in Table 1.

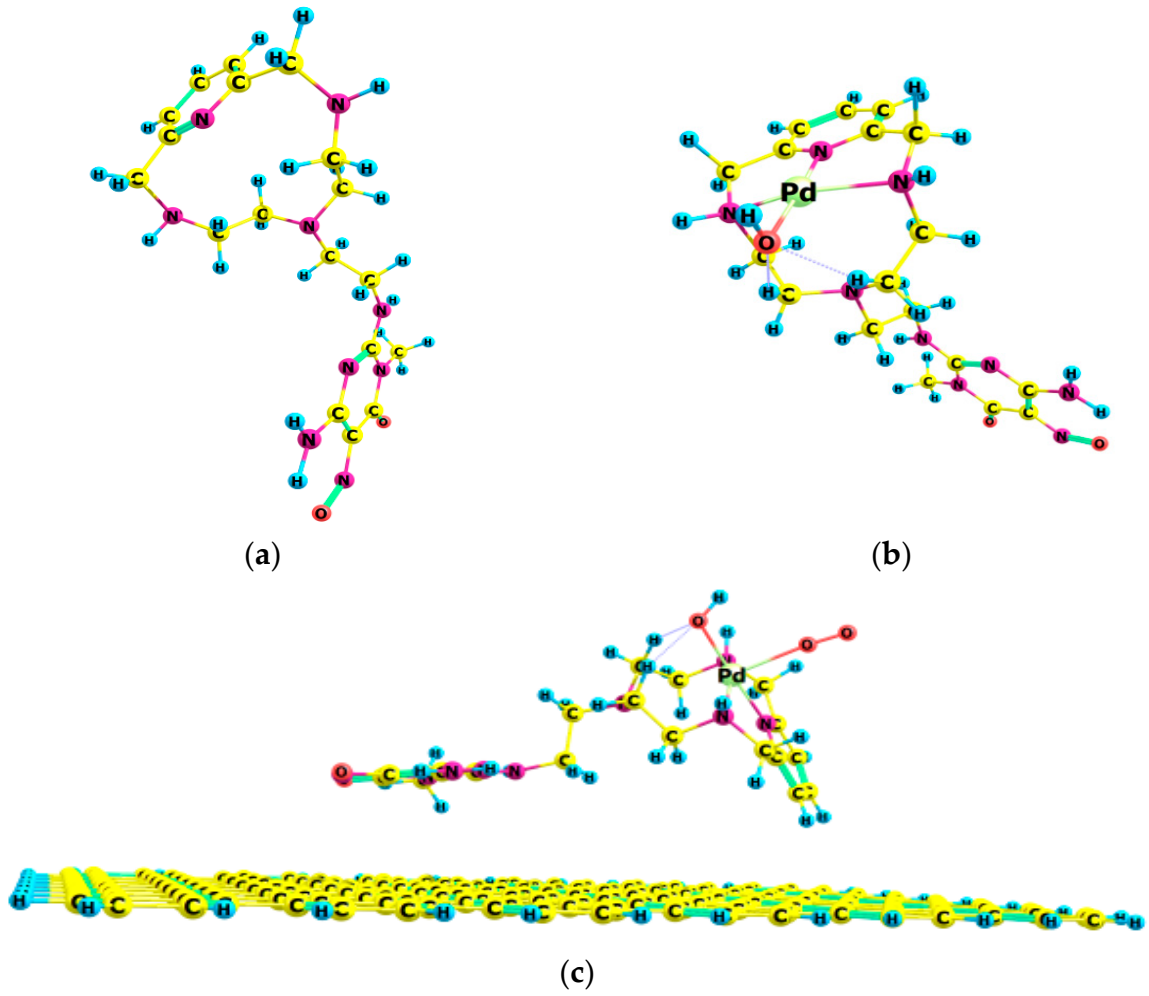

Figure 1. Molecular structures for the ORR catalyst: (**a**) HL1 (**b**); HL1-Pd(II)-OH^- complex; (**c**) Cat1 final adduct C2D-HL1-Pd(II)-OH^- with O_2 interaction.

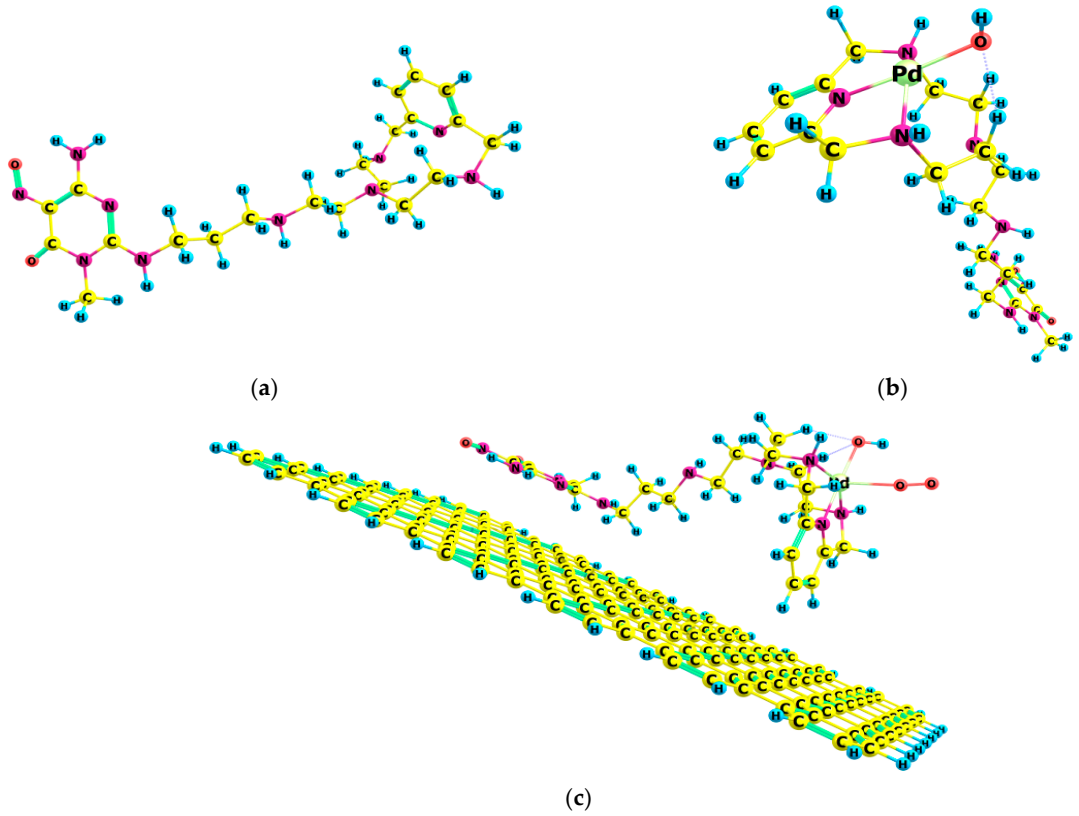

Figure 2. Molecular structures for the ORR catalyst: (**a**) HL2; (**b**) HL2-Pd(II)-OH^- complex; (**c**) Cat2 final adduct C2D-HL2-Pd(II)-OH^- with O_2 interaction.

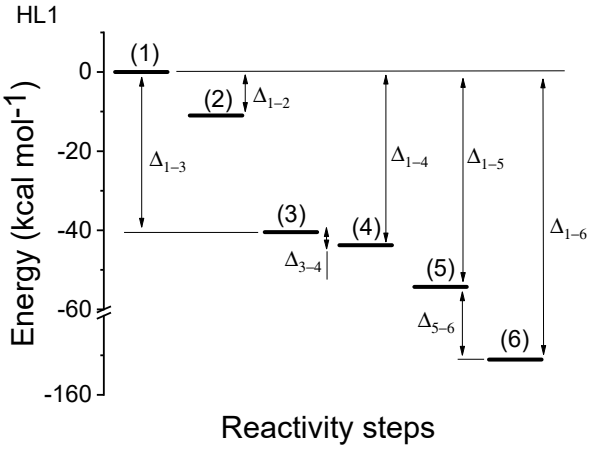

Figure 3. Potential energy surface (PES) for the elementary reactions yielding the composite catalyst: 1 to 5 (Cat1). Energy difference 6 corresponds to the catalyst/oxygen interaction, in the case of the HL1 supramolecular catalyst, UHF PM6 level of theory (compare Table 1 and Results and Discussion section for the details). SCF energy of (1) $Energy_{C2D} + Energy_{HL1} + Energy_{Pd(II)} + Energy_{OH^-} + Energy_{O_2}$, (2) $Energy_{C2D-HL2} + Energy_{Pd(II)} + Energy_{OH^-} + Energy_{O_2}$, (3) $Energy_{C2D} + Energy_{HL2-Pd(II)-OH^-} + Energy_{O_2}$, (4) $Energy_{C2D} + Energy_{HL2-Pd(II)-OH^- - O_2}$, (5) $Energy_{C2D-HL2-Pd(II)-OH^-} + Energy_{O_2}$, (6) $Energy_{C2D-HL2-Pd(II)-OH^- - O_2}$. The energy level (1) represents the sum of the energies of the non-interacting species, while (6) represents the energy of the complete catalyst supermolecule. The energy of the O_2 molecule was calculated in the electronic triplet state. The energy levels of the six steps have been normalized to the energy of state (1), which corresponds to a 748.42 kcal mol^{-1} absolute value.

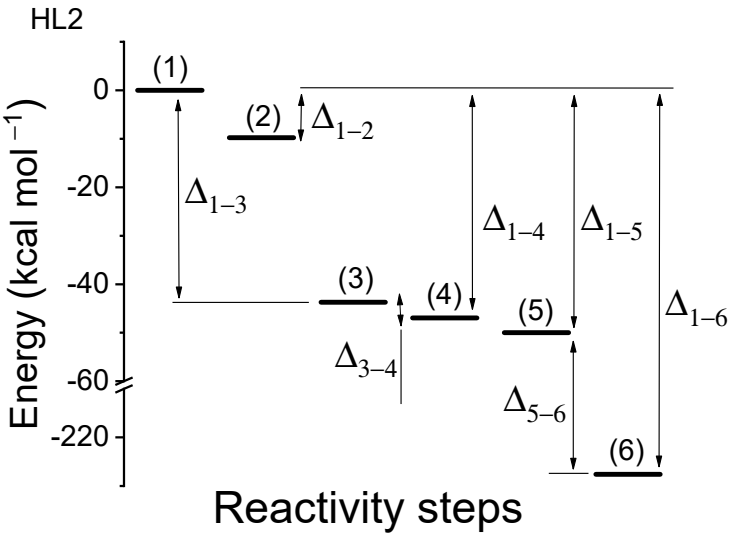

Figure 4. Potential energy surface (PES) for the elementary reactions yielding the composite catalyst: 1 to 5 (Cat2). Energy difference 6 corresponds to the catalyst/oxygen interaction, in the case of the HL2 supramolecular catalyst, UHF PM6 level of theory (compare Table 1 and Results and Discussion section for the details). SCF energy of (1) $Energy_{C2D} + Energy_{HL2} + Energy_{Pd(II)} + Energy_{OH^-} + Energy_{O_2}$, (2) $Energy_{C2D-HL2} + Energy_{Pd(II)} + Energy_{OH^-} + Energy_{O_2}$, (3) $Energy_{C2D} + Energy_{HL2-Pd(II)-OH^-} + Energy_{O_2}$, (4) $Energy_{C2D} + Energy_{HL2-Pd(II)-OH^- - O_2}$, (5) $Energy_{C2D-HL2-Pd(II)-OH^-} + Energy_{O_2}$, (6) $Energy_{C2D-HL2-Pd(II)-OH^- - O_2}$. The energy level (1) represents the sum of the energies of the non-interacting species, while (6) represents the energy of the complete catalyst supermolecule. The energy of the O_2 molecule was calculated in the electronic triplet state. The energy levels of the six steps have been normalized to the energy of state (1), which corresponds to a 744.78 kcal mol^{-1} absolute value.

Table 1. Interaction energies of reactivity steps of Cat1 and Cat2 supramolecular catalysts.

Inter-Molecular Interaction †		Cat1 kcal mol^{-1}	Cat2 kcal mol^{-1}
Ligand adsorption on C2D Δ1–2	Δ1–2	−10.99	−9.77
Ligand Pd(II) OH^- complexation	Δ1–3	−40.46	−43.71
Adduct adsorption on C2D	Δ1–4	−43.77	−46.97
Ligand O_2 absorption	Δ3–4	−3.31	−3.26
Adduct stability	Δ1–5	−54.29	−49.98
Adduct O_2 absorption	Δ5–6	−96.79	−177.64
Adduct O_2 stability	Δ1–6	−151.09	−227.62

† Compare the Results and Discussion section and Figures 3 and 4 for the relevant details.

A very large variation in MO energies is found as a function of the molecular architecture. The presence of a graphitic-like plane simulating the surface of MWCNT drastically changes the MO energy hierarchy, giving due count to the experimental efficiency found for the more complex molecular structure. Full details concerning MO energy diagrams are shown in Supporting Information.

The energy ordering and shape of virtual orbitals for the HL1 moiety, Cat1, suggest that an electron "hopping" mechanism could explain the catalytic effect observed. Electrons can hop from the surface of the nanotube to the palladium complex to which the oxygen molecule is adsorbed, as can be seen in Figure 5.

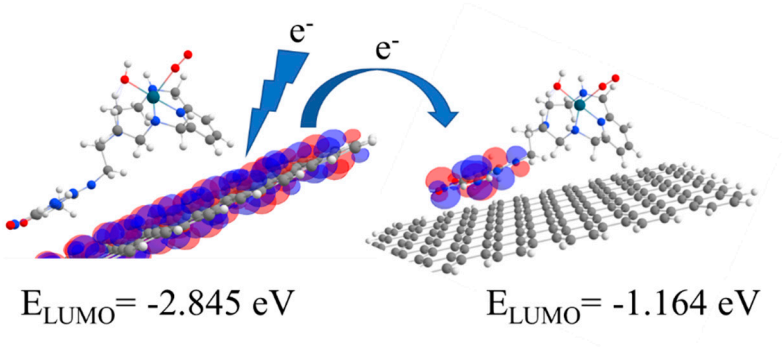

Figure 5. Scheme representing the ORR process on a functionalized carbon nanotube.

There is a difference in the LUMO energy between Cat1 and Cat2 superstructures: −3.486 and −3.514 eV, respectively. Note that the same does not hold for the HOMO, compare LUMO energy value of C2D-HL1-Pd(II)-OH and C2D-HL1-Pd(II)-OH in Tables S1 and S2.

When the isolated HL-Pd(II)-OH-O2 (L = L1, L2) super-structures are considered, both show a LUMO centered on the pyrimidine anchoring group and LUMO+1 and +2 levels centered on the coordinating pyridine moiety (with significant more involvement of the metal center in the LUMO+2 level in the case of HL2) (cf. Supporting Information). Arguably, the insertion of an aromatic ligand, such as pyridine, with respect to alkyl amines alternatives, leads to a reduced LUMO-LUMO+1 gap, and thus to improved electron injection from the anchoring pyrimidine towards the metal active site. This overall suggests the possibility to actively engineer related system on the basis of the relative energies of anchoring group and aromatic ligand/Pd(II) complex orbitals. Ligands with less spatial separation between the anchoring and metal-binding moiety [25] could also be considered.

The most interesting results are obtained by considering the OM energies of the reduced species. For the reduced species, the doublet and quartet spin multiplicity states were considered, and Table 2 shows a summary of the four MOs energy values around the HOMO-LUMO gap. A much more extended table is presented in the Supporting Information (Tables S1 and S2).

Table 2. Orbitals energies of Cat1 and Cat2 value in eV. Spatial location of orbital is assigned with letters a—pyrimidine anchorage site, b—spacer group, c—macrocyle, d—pyridine, e—Palladium, f—hydroxyl anion, g—Oxygen, h—C2D carbon surface. Reduced $2e^-$ species are calculated from reduced $1e^-$ with single-point energy calculations. Alfa OM energies are reported in the case of unrestricted calculation. For a more detailed table, see Supporting Information.

	Reduced 1e⁻				**Reduced 2e⁻**			
Orbitals	**C2D-HL1-Pd(II)-OH-O2 (2)**		**C2D-HL1-Pd(II)-OH-O2 (4)**		**C2D-HL1-Pd(II)-OH-O2 (3)**		**C2D-HL1-Pd(II)-OH-O2 (1)**	
				eV				
HOMO −1	−7.877	e,f	−7.529	e,f,g	−7.929	e,f,g	−6.899	h
HOMO	−7.611	g	−6.233	d	−6.603	h	−5.918	h,a,d
LUMO	−1.987	h	−3.049	h	−2.054	h	−4.719	h
LUMO +1	−1.948	h	−2.263	h	−1.679	h,a	−3.008	h,a
Orbitals	**C2D-HL2-Pd(II)-OH-O2 (2)**		**C2D-HL2-Pd(II)-OH-O2 (4)**		**C2D-HL2-Pd(II)-OH-O2 (3)**		**C2D-HL2-Pd(II)-OH-O2 (1)**	
				eV				
HOMO −1	−7.903	e,f,g	−7.491	c,e,f,g	−7.491	e,f,g	−6.958	h
HOMO	−6.036	h	−6.177	d,e	−7.428	h	−6.884	h
LUMO	−1.900	h	−3.052	h	−3.624	h	−3.495	h,a
LUMO +1	−1.733	h	−2.269	h	−2.684	h,a	−2.938	h,a

Among mono-reduced species, Cat1 − O_2 (doublet state) is the most stable; it has the lowest LUMO energy (−1.987 eV compared to −1.900 eV for Cat2 − O_2). In the case of HL1 in the structure obtained by full optimisation, it is observed that the oxygen molecule dissociates from the complex as O_2^- (the total negative charge is found on the oxygen). The resulting superoxide anion can increase the production of hydrogen peroxide, as observed by experimental data. The two catalysts feature catalytic activity comparable to those of an

expensive Pt electrode: Cat1 shows an onset potential of +0.91 V vs. RHE, whereas Cat2 shows a value of +0.95 V. The greatest differences between the two systems are observed with regard to the direct production of H_2O: the ORR process, Cat2 working electrode, is a four electrons process, whereas Cat1 promotes greater production of hydrogen peroxide. Among $2e^-$ reduced species, $Cat2 - O_2$ is the most stable as it has molecular orbital energies of less than approximately 1 eV. The reduced species have a molecular geometry very similar to that of the original species, so the reduction does not involve any significant changes in the structure of the ligands, which may explain the high stability in successive reduction cycles observed experimentally. All in all, the energy of LUMO ordering Cat1 vs. Cat2 gives due reason to the experimental outcome, where the most effective catalytic capability is shown by Cat2.

4. Computational Details/Methods

Due to the sizable molecular structures here considered, all the theoretical results here reported concern species in all possible oxidation states, and spin multiplicity is performed in the framework of semi-empirical quantum mechanical based methods: PM6 Hamiltonian. In the calculations, the structure of the CNTs was approximated by a perfectly flat, two-dimensional 6×7 (aromatic rings) 2D carbon structure (C2D), in order to reduce the system complexity to a feasible degree. All calculations were performed using C1 symmetry and unrestricted wave function using the Gaussian 16 program [26]. The Chemcraft program [27] is used for visualization purposes, for both molecular structures and molecular orbitals display. Molecular geometries are obtained by full optimization carried out at UHF PM6 levels of the theory. To account for solute−solvent interaction, geometry optimization is carried out using Barone and Cossi's polarizable conductor model (CPCM) [28,29].

5. Conclusions

In this paper, we modelled theoretically the catalytic activity of two composite catalysts. These were obtained by suitably functionalized carbon nanotubes, using Pd(II) complexes. Indeed, functionalized carbon nanotubes (in this paper approximated by an ideally flat 2D-carbon sheet), proved to be an effective alternative to classical Pt-based catalysts [11].

In particular, the essential features of the ORR process are accounted for by considering them as a sequence of four elementary steps, which we showed to correspond to a down-hill in energy PES: compare Table 1 and Figures 3 and 4. Our theoretical results also show that VdW forces (physical interaction) are responsible for the stability of the intermolecular Pd complex@2D-carbon "supramolecular system" (π-π stacking): -13.8 and -6.3 kcal mol^{-1}, for HL1 and HL2, respectively.

The total supramolecular stabilization energies are -151 and -228 kcal mol^{-1} for Cat1 and Cat2, respectively. What is more, the ordering of LUMOs energies suggests that an electron "hopping" mechanism is consistent with the observed catalytic effect: the electron uptake involves, *in primis*, the C2D structure followed by a transfer on a virtual orbital localized on the Pd(II) complex.

The reaction mechanism here proposed, and the relevant theoretical results obtained by using the PM6 semiempirical Hamiltonian, give due count to the experimental evidence of a more efficient ORR process based on the use of the HL2 complex molecular architectures. Remarkably, the oxygen/Pd(II)-complex stabilization energies are -96.79 and -177.64 kcal mol^{-1} for Cat1 and Cat2, respectively.

Moreover, a few insightful pieces of information emerged from the data. First, an ancillary ligand on the Pd(II) center is not mandatory for ORR, as O_2 can still bind to the metal ion via an axial bond; this simplifies ligand design. Second, the energy of unoccupied molecular orbitals involving the metal center and/or its aromatic ligand, with respect to the anchoring group-centered LUMO, might play a significant role. While this is not a

direct simplification of the preparation of such a system, it surely offers space to make informed design choices.

Thus, the mechanism here proposed, in terms of single elementary steps, sheds light on the role played by single-atom catalysts (SACs) in the ORR overall process.

Supplementary Materials: The following are available online at https://www.mdpi.com/article/10.3390/catal11070764/s1: Further details are reported concerning molecular orbital energies. Table S1: Molecular orbitals energies of HL1 catalyst. Table S2: Molecular orbitals energies of HL2 catalyst. Figure S1: Molecular Orbital energies diagram for HL1 catalyst. Figure S2: Molecular Orbital energies diagram for HL1 catalyst.

Author Contributions: Conceptualization, C.F.; software M.B. and C.F.; writing—original draft preparation, M.B., M.S., and C.F.; writing—review and editing, W.G., M.S., M.V. and A.S.; supervision, A.B. and M.I.; funding acquisition, M.I. All authors have read and agreed to the published version of the manuscript.

Funding: This research was funded by the PRIN ("Progetti di Ricerca di Rilevante Interesse Nazionale"), which made possible the project "Novel Multilayered and Micro-Machined Electrode Nano-Architectures for Electrocatalytic Applications (Fuel Cells and Electrolyzers)", grant number 2017YH9MRK.

Institutional Review Board Statement: Not applicable.

Informed Consent Statement: Not applicable.

Conflicts of Interest: The authors declare no conflict of interest.

References

1. Zheng, S.; Jiujun, Z. Density functional theory study of transitional metal macrocyclic complexes' dioxygen-binding abilities and their catalytic activities toward oxygen reduction reaction. *J. Phys. Chem. C* **2007**, *111*, 7084–7090. [CrossRef]
2. He, H.; Lei, Y.; Xiao, C.; Chu, D.; Chen, R.; Wang, G. Molecular and electronic structures of transition-metal macrocyclic complexes as related to catalyzing oxygen reduction reactions: A density functional theory study. *J. Phys. Chem. C* **2012**, *116*, 16038–16046. [CrossRef]
3. Savastano, M.; Passaponti, M.; Giurlani, W.; Lari, L.; Calisi, N.; Delgado-Pinar, E.; Serrano, E.S.; Garcia-España, E.; Innocenti, M.; Lazarov, V.K.; et al. Linear, tripodal, macrocyclic: Ligand geometry and ORR activity of supported Pd(II) complexes. *Inorg. Chim. Acta* **2021**, *518*, 120250. [CrossRef]
4. Savastano, M.; Passaponti, M.; Giurlani, W.; Lari, L.; Bianchi, A.; Innocenti, M. Multi-Walled Carbon Nanotubes Supported Pd(II) Complexes: A Supramolecular Approach towards Single-Ion Oxygen Reduction Reaction Catalysts. *Energies* **2020**, *13*, 5539. [CrossRef]
5. Savastano, M.; Arranz-Mascarós, P.; Bazzicalupi, C.; Clares, M.P.; Godino-Salido, M.L.; Guijarro, L.; Gutiérrez-Valero, M.D.; Bianchi, A.; García-España, E.; López-Garzón, R. Polyfunctional Tetraaza-Macrocyclic Ligands: Zn(II), Cu(II) Binding and Formation of Hybrid Materials with Multiwalled Carbon Nanotubes. *ACS Omega* **2017**, *2*, 3868–3877. [CrossRef]
6. Passaponti, M.; Rosi, L.; Frediani, M.; Salvietti, E.; de Luca, A.; Giaccherini, A.; Innocenti, M. Microwave Assisted Pyrolysis of Waste Tires: Study and Design of Half-Cells SOFCs with Low Environmental Impact. *ECS Trans.* **2017**, *78*, 1933–1940. [CrossRef]
7. Passaponti, M.; Rosi, L.; Savastano, M.; Giurlani, W.; Miller, H.A.; Lavacchi, A.; Filippi, J.; Zangari, G.; Vizza, F.; Innocenti, M. Recycling of waste automobile tires: Transforming char in oxygen reduction reaction catalysts for alkaline fuel cells. *J. Power Sources* **2019**, *427*, 85–90. [CrossRef]
8. Passaponti, M.; Lari, L.; Bonechi, M.; Bruni, F.; Giurlani, W.; Sciortino, G.; Rosi, L.; Fabbri, L.; Vizza, M.; Lazarov, V.K.; et al. Optimisation Study of Co Deposition on Chars from MAP of Waste Tyres as Green Electrodes in ORR for Alkaline Fuel Cells. *Energies* **2020**, *13*, 5646. [CrossRef]
9. An, Y.; Tian, Y.; Zhang, Y.; Wei, C.; Tan, L.; Zhang, C.; Cui, N.; Xiong, S.; Feng, J.; Qian, Y. Two-Dimensional Silicon/Carbon from Commercial Alloy and CO_2 for Lithium Storage and Flexible $Ti_3C_2T_x$ MXene-Based Lithium–Metal Batteries. *ACS Nano* **2020**, *14*, 17574–17588. [CrossRef]
10. Wang, D.-W.; Su, D. Heterogeneous nanocarbon materials for oxygen reduction reaction. *Energy Environ. Sci.* **2014**, *7*, 576. [CrossRef]
11. Passaponti, M.; Savastano, M.; Clares, M.P.; Inclán, M.; Lavacchi, A.; Bianchi, A.; García-España, E.; Innocenti, M. MWCNTs-Supported Pd(II) Complexes with High Catalytic Efficiency in Oxygen Reduction Reaction in Alkaline Media. *Inorg. Chem.* **2018**, *57*, 14484–14488. [CrossRef]
12. Savastano, M.; Arranz-Mascarós, P.; Bazzicalupi, C.; Clares, M.P.; Godino-Salido, M.L.; Gutiérrez-Valero, M.D.; Inclán, M.; Bianchi, A.; García-España, E.; López-Garzón, R. Construction of green nanostructured heterogeneous catalysts via non-covalent surface decoration of multi-walled carbon nanotubes with Pd(II) complexes of azamacrocycles. *J. Catal.* **2017**, *353*, 239–249. [CrossRef]

13. Kolthoff, I.M. The Oxidation States of the Elements and their Potentials in Aqueous Solutions. By W.M. Latimer. *J. Phys. Chem.* **1939**, *43*, 396. [CrossRef]
14. Katsounaros, I.; Schneider, W.B.; Meier, J.C.; Benedikt, U.; Biedermann, P.U.; Cuesta, A.; Auer, A.A.; Mayrhofer, K.J.J. The impact of spectator species on the interaction of H_2O_2 with platinum—Implications for the oxygen reduction reaction pathways. *Phys. Chem. Chem. Phys.* **2013**, *15*, 8058. [CrossRef]
15. Sala, X.; Maji, S.; Bofill, R.; García-Antón, J.; Escriche, L.; Llobet, A. Molecular Water Oxidation Mechanisms Followed by Transition Metals: State of the Art. *Acc. Chem. Res.* **2014**, *47*, 504–516. [CrossRef]
16. Ma, R.; Lin, G.; Zhou, Y.; Liu, Q.; Zhang, T.; Shan, G.; Yang, M.; Wang, J. A review of oxygen reduction mechanisms for metal-free carbon-based electrocatalysts. *Npj Comput. Mater.* **2019**, *5*. [CrossRef]
17. Mtangi, W.; Kiran, V.; Fontanesi, C.; Naaman, R. Role of the Electron Spin Polarization in Water Splitting. *J. Phys. Chem. Lett.* **2015**, *6*, 4916–4922. [CrossRef]
18. Mtangi, W.; Tassinari, F.; Vankayala, K.; Vargas Jentzsch, A.; Adelizzi, B.; Palmans, A.R.A.; Fontanesi, C.; Meijer, E.W.; Naaman, R. Control of Electrons' Spin Eliminates Hydrogen Peroxide Formation During Water Splitting. *J. Am. Chem. Soc.* **2017**, *139*, 2794–2798. [CrossRef]
19. Gazzotti, M.; Arnaboldi, S.; Grecchi, S.; Giovanardi, R.; Cannio, M.; Pasquali, L.; Giacomino, A.; Abollino, O.; Fontanesi, C. Spin-dependent electrochemistry: Enantio-selectivity driven by chiral-induced spin selectivity effect. *Electrochim. Acta* **2018**, *286*, 271–278. [CrossRef]
20. Gazzotti, M.; Stefani, A.; Bonechi, M.; Giurlani, W.; Innocenti, M.; Fontanesi, C. Influence of Chiral Compounds on the Oxygen Evolution Reaction (OER) in the Water Splitting Process. *Molecules* **2020**, *25*, 3988. [CrossRef]
21. Lu, Z.; Chen, G.; Siahrostami, S.; Chen, Z.; Liu, K.; Xie, J.; Liao, L.; Wu, T.; Lin, D.; Liu, Y.; et al. High-efficiency oxygen reduction to hydrogen peroxide catalysed by oxidized carbon materials. *Nat. Catal.* **2018**, *1*, 156–162. [CrossRef]
22. Song, C.; Zhang, J. Electrocatalytic oxygen reduction reaction. In *PEM Fuel Cell Electrocatalysts and Catalyst Layers: Fundamentals and Applications*; Springer Science & Business Media: Berlin/Heidelberg, Germany, 2008; ISBN 9781848009356.
23. Pang, Y.; Xie, H.; Sun, Y.; Titirici, M.-M.; Chai, G.-L. Electrochemical oxygen reduction for H_2O_2 production: Catalysts, pH effects and mechanisms. *J. Mater. Chem. A* **2020**, *8*, 24996–25016. [CrossRef]
24. Savastano, M.; Arranz-Mascarós, P.; Clares, M.P.; Cuesta, R.; Godino-Salido, M.L.; Guijarro, L.; Gutiérrez-Valero, M.D.; Inclán, M.; Bianchi, A.; García-España, E.; et al. A New Heterogeneous Catalyst Obtained via Supramolecular Decoration of Graphene with a Pd^{2+} Azamacrocyclic Complex. *Molecules* **2019**, *24*, 2714. [CrossRef] [PubMed]
25. Savastano, M.; Zoppi, C.; Bianchi, A.; Bazzicalupi, C. Synthesis and coordination properties of a new ligand designed for surface functionalization of carbon substrates. *Inorg. Chim. Acta* **2020**, *511*, 119793. [CrossRef]
26. Pople, J. *Gaussian Suite of Programs*; Gaussian, Inc.: Wallingford, CT, USA, 2017.
27. Chemcraft-Graphical Software for Visualization of Quantum Chemistry Computations. Available online: https://www.chemcraftprog.com (accessed on 23 June 2021).
28. Barone, V.; Cossi, M. Quantum Calculation of Molecular Energies and Energy Gradients in Solution by a Conductor Solvent Model. *J. Phys. Chem. A* **1998**, *102*, 1995–2001. [CrossRef]
29. Miertuš, S.; Scrocco, E.; Tomasi, J. Electrostatic interaction of a solute with a continuum. A direct utilizaion of AB initio molecular potentials for the prevision of solvent effects. *Chem. Phys.* **1981**, *55*, 117–129. [CrossRef]